Nonstoichiometry accommodation in $SrTiO_3$ thin films studied by positron annihilation and electron microscopy

D. J. Keeble,[1,*] S. Wicklein,[2] L. Jin,[2] C. L. Jia,[2] W. Egger,[3] and R. Dittmann[2,*]

[1]*Carnegie Laboratory of Physics, SUPA, School of Engineering, Physics, and Mathematics, University of Dundee, Dundee DD1 4HN, United Kingdom*

[2]*Peter Grünberg Institute, Forschungszentrum Jülich, 52425 Jülich, Germany*

[3]*Institut für Angewandte Physik und Messtechnik, Universität Bundeswehr München, D-85577 Neubiberg, Germany*

(Received 31 December 2012; revised manuscript received 25 March 2013; published 8 May 2013)

Accommodation of nonstoichiometry in $SrTiO_3$ pulsed laser deposited (PLD) films was investigated using positron annihilation lifetime spectroscopy and (scanning) transmission electron microscopy. Increasing PLD laser fluence changed the stoichiometry from Ti to Sr deficient. Cation vacancy defects were detected, and the concentration ratio of Sr to Ti vacancies, $[V_{Sr}]/[V_{Ti}]$, was observed to increase systematically in the Sr-deficient region, although no change in the electron microscopy lattice images was detected. Increasing Ti deficiency resulted in the accommodation of SrO layers in planar defects, and in the formation of vacancy cluster defects. A change from V_{Ti} to V_{Sr} defect positron trapping was also detected.

DOI: 10.1103/PhysRevB.87.195409 PACS number(s): 68.55.Ln, 77.84.−s, 78.70.Bj

I. INTRODUCTION

Strontium titanate is a model perovskite oxide, ABO_3, material of central importance for both fundamental studies and for the developing field of oxide electronics. Epitaxial multilayers with well-defined interfaces can be grown with a wide variety of other ABO_3 materials exhibiting a diverse range of physical properties. New phenomena such as the improper ferroelectricity,[1] and most notably the formation of a two-dimensional electron gas at the interface between $SrTiO_3$ and other band insulator oxides,[2,3] have been demonstrated from heteroepitaxial structures. The role of perovskite oxides as emergent research device materials will impose additional severe demands on stoichiometry and impurity content;[4] while these are routine considerations for traditional device materials, they have generally been of secondary importance for oxides. High-quality epilayers of perovskite oxides are normally deposited either by pulsed laser deposition (PLD) or molecular beam epitaxy (MBE). It was initially assumed that transfer of stoichiometry from target to film in the PLD process readily occurred; however, Dam *et al.* and Ohnishi *et al.*[5–8] established that this can only be achieved for a restricted range deposition conditions, for example, laser energy density (fluence). Nonideal conditions normally result in films with a measureable expansion of the out-of-plane lattice parameter, Δc. Recently, PLD-grown $SrTiO_3$ films with $\Delta c \sim 0$ have been obtained using growth temperatures (T_g) above 1000 °C, while the mobility peaked for $T_g \sim 1200$ °C; this was attributed to a suppression of Sr and oxygen vacancies.[9]

An understanding of the accommodation of nonstoichiometry is developing, but it is incomplete.[10–13] Direct experimental evidence on the nature of point defects and their role is particularly lacking. For PLD, the physical mechanisms contributing to the growth process may often dominate equilibrium processes and so strongly influence defect content.[14,15]

This work utilized the atomic-scale defect characterization method positron annihilation lifetime spectroscopy (PALS) to identify the nature of vacancy-related defects in a sequence of PLD-grown homoepitaxial $SrTiO_3$ thin films deposited with varying laser fluence, F. Both Ti and Sr vacancies are observed in all the films, and a systematic variation in positron trapping from Ti vacancy–dominated to Sr vacancy–dominated trapping is observed as F is increased from the optimal value, F_o. Films grown using fluences below F_o, in the Ti-poor regime, also contain vacancy cluster defects. Changes in microstructure were observed using high-angle annular dark-field (HAADF) imaging, based on scanning transmission electron microscopy (STEM), and using the high-resolution transmission electron microscopy (HRTEM) technique.

A. Thin film $SrTiO_3$ nonstoichiometry

Previous studies of thin film $SrTiO_3$, grown by various methods, have established the variation in out-of-plane lattice expansion, Δc, with Ti/Sr ratio shown in Fig. 1.[6,8,10–12,16,17] Film compositions have been determined by energy-dispersive x-ray spectroscopy (EDX), Rutherford backscattering spectrometry, or x-ray photoelectron spectroscopy measurements.[12,17] The behavior of Δc with Ti/Sr is consistent, but quite marked variations in the magnitudes of expansion are reported. For PLD-grown films, the variation in stoichiometry can be achieved by varying the laser fluence, F.[5–8] Increasing F initially results in decreasing Δc up to an optimal value, F_o, where $\Delta c \sim 0$ can be obtained; increasing F further results in an increase in Δc (see Fig. 2).[6,8,10–12,18] Composition analysis measurements show that films grown with fluences lower than F_o are Ti deficient, while films grown with higher values are Sr deficient.[10–12] The specific value of F_o has been observed to be system dependent, but it is typically in the 0.3–1.5 J cm^{-2} range.

Small deviations from stoichiometry are expected to be accommodated by the formation of point defects. Strontium vacancies have been considered previously, but Ti vacancies have generally been ignored due to the higher formation energies obtained from calculations.[19] Both types of cation vacancy are expected to degrade the electrical properties,[8,9,12,13] and thermal conductivity,[12,20,21] of the $SrTiO_3$ layers. The effect of nonstoichiometry on carrier concentrations and mobilities in PLD-grown donor-doped thin films has been studied by several groups.[8,9,13] The dielectric measurements on undoped

 ©2013 American Physical Society

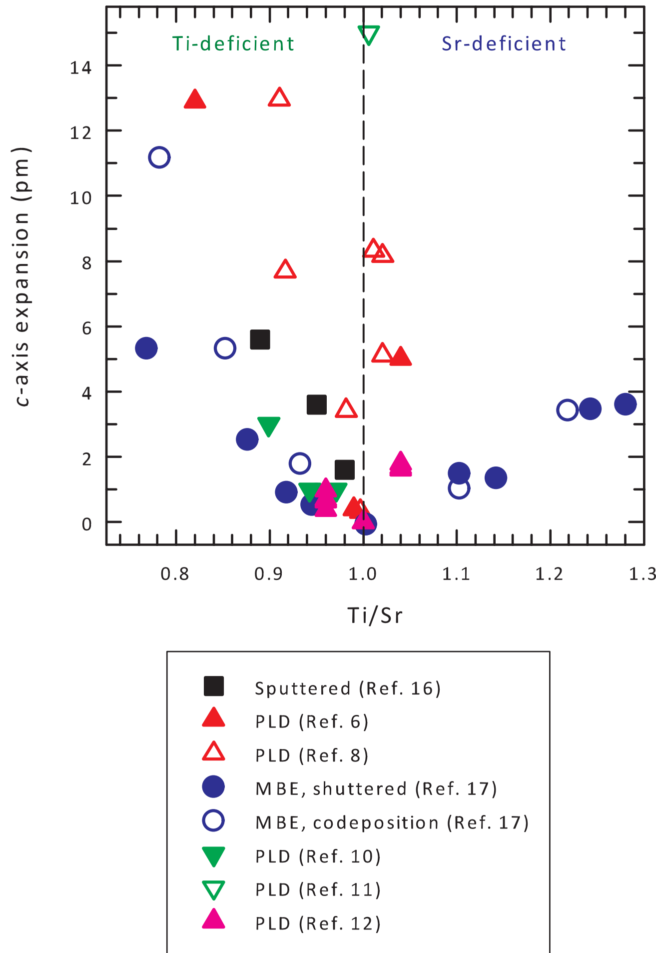

FIG. 1. (Color online) $SrTiO_3$ thin film out-of-plane lattice parameter expansion, measured by x-ray diffraction, as a function of Ti/Sr ratio.

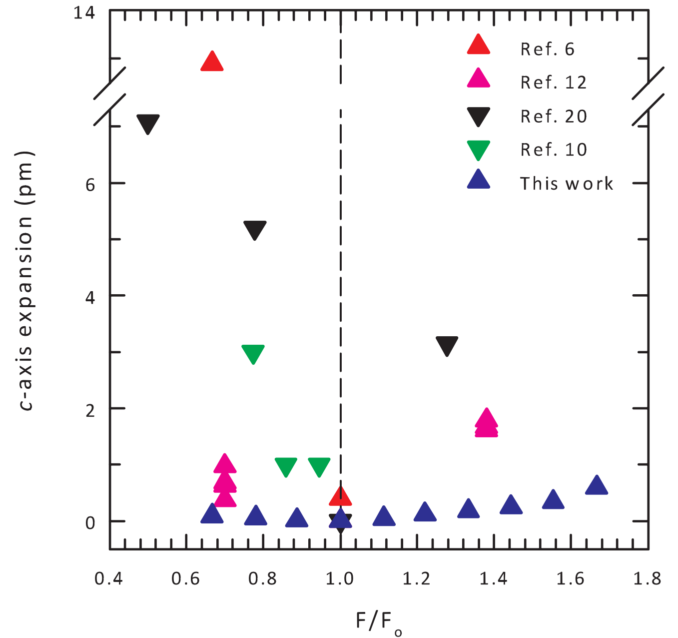

FIG. 2. (Color online) Pulsed laser deposited $SrTiO_3$ thin film out-of-plane lattice parameter expansion against the ratio of laser fluence, F, to optimal fluence, F_o. The values from Ref. 20 were obtained for an oxygen partial pressure of 0.1 Torr.

PLD-grown $SrTiO_3$, as a function of nonstoichiometry, reported a decrease in the dielectric constant with increasing nonstoichiometry, with the largest depression for the Ti-deficient films, and an increase in the loss tangent, with the largest increases observed for the Sr-deficient films.[12]

TEM studies of Ti-deficient $SrTiO_3$ have identified extended crystallographic shear (CS) plane defects resulting from coherent intergrowth of various $Sr_{n+1}Ti_nO_{3n+1}$ Ruddlesden-Popper (RP) phases.[16,22,23] Subsequently, extended RP planar faults that result from the insertion of additional SrO layers were observed in Ti-deficient thin films grown by both PLD and MBE.[6,8,10,17] For strongly Sr-deficient films, precipitates of the TiO_2 amorphous phase have been observed.[22] Films grown with Ti/Sr > 1, but below the threshold for the precipitation of amorphous TiO_2 occlusions, tend to exhibit wide-area inhomogeneous contrast modulations in HRTEM or STEM images, attributed to disordered structure resulting from the presence of point defects.[8,11,17]

B. Positron annihilation spectroscopy

Implanted positrons rapidly thermalize and then annihilate from a state i with a lifetime τ_i and probability I_i.[24] This can be a delocalized state in a perfect lattice, or one localized at a vacancy defect, since positrons can trap strongly in the potential well resulting from the missing atomic core. The reduced electron density at the vacancy site increases the positron lifetime above the value characteristic of the perfect (bulk) material, τ_b (Table I). If vacancy defects are present, the average lifetime detected, $\bar{\tau} = \sum_i I_i \tau_i$, is greater than the bulk lifetime, and this typically provides a robust, fitting-independent, parameter. The rate of positron trapping to a vacancy defect, κ_d, is proportional to the defect concentration, $[d]$, and the constant of proportionality is the defect-specific trapping coefficient, μ_d. The one-defect standard trapping model (1D-STM) predicts two experimental positron lifetime components: The second has a fixed value characteristic of the positron trapping defect, $\tau_2 = \tau_d$, and the first has a value reduced below the bulk lifetime, $\tau_1 \leqslant \tau_b$, by an amount that depends on the rate of trapping to the defect, κ_d, which is given by the expression[24]

$$\kappa_d = \mu_d\,[d] = I_2\left(\frac{1}{\tau_1} - \frac{1}{\tau_2}\right). \tag{1}$$

The model is readily extended to more than one defect. This results in the appropriate number of fixed lifetime components, with values characteristic of the defects, and a reduced bulk component with a lifetime and intensity that reduce with increasing defect trapping.

TABLE I. Positron lifetime values (ps) calculated by the DFT method MIKA for monovacancies from Ref. 29 and for vacancy complexes from Ref. 28 in $SrTiO_3$.

Bulk	V_{Ti}	V_{Sr}	V_O	V_{Ti-O}	V_{Sr-O}	V_{Sr-3O}	$V_{Ti-3O-Sr}$
152	189	281	161	225	283	289	316

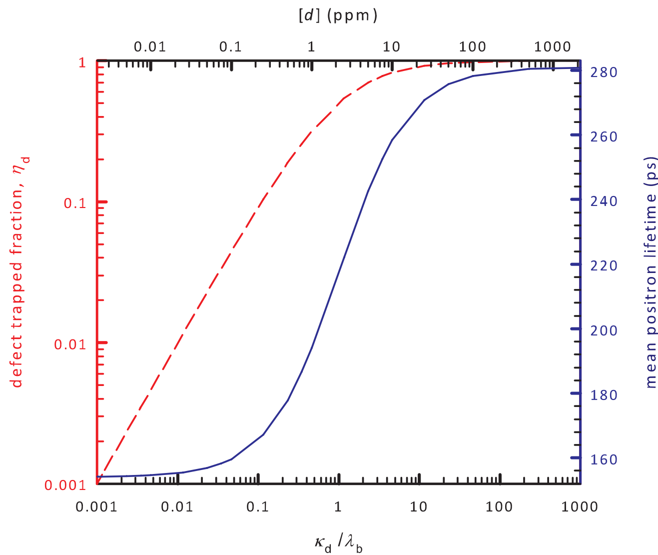

FIG. 3. (Color online) The one-defect standard trapping model calculated variation in the defect trapped fraction with defect concentration, $[d]$, and positron trapping rate, κ_d, assuming $\mu_d = 3 \times 10^{15}$ s^{-1} and $1/\lambda_b = 154$ ps (red dashed line). The associated behavior of the mean positron lifetime, assuming a defect lifetime of 281 ps, is also shown (blue solid line).

Saturation trapping initiates when the concentration of vacancy defects increases to the point where the large majority of positrons annihilate from the defects; the reduced bulk lifetime intensity becomes negligible, and its lifetime value is too short to detect. The saturation trapping limit is indicated by the condition, $\mu_d\,[d]_{Sat}\,\tau_b \approx 10$. The variation of the trapped fraction with defect concentration is illustrated in Fig. 3, applying the 1D-STM, and the associated variation in mean positron lifetime is also given. It should, however, be noted that no direct determination of μ_d for a vacancy defect in an oxide has been made, but room temperature values for negatively charged vacancy defects in various semiconductors have been estimated to be in the range 0.1–29 $\times 10^{15}$ s^{-1}.[24] If the more typical value $\mu_d \sim 2 \times 10^{15}$ s^{-1} is assumed, then saturation trapping should initiate for defect concentrations greater than ~50 ppm.

If trapping is dominated by two defects, and the concentrations are above the saturation trapping threshold, two lifetime components with values characteristic of the two types of defects are predicted. The ratio of the intensities of the two lifetime components is given by the expression

$$\frac{I_2}{I_1} = \frac{\kappa_{d2}}{\kappa_{d1}} = \frac{\mu_{d2}\,[d_2]}{\mu_{d1}\,[d_1]}, \tag{2}$$

and it is proportional to the ratio of the defect concentrations, with a constant of proportionality given by the ratio of the defect-specific trapping coefficients. For defects in insulators or semiconductors, the defect-specific trapping coefficient values depend on the relative charge of the trapping center with respect to the lattice. The Coulomb barrier presented by positively charged defects normally results in negligible trapping rates; however, neutral or negatively charged vacancy-related defects are effective positron traps.[24]

The dominant native point defects in the close-packed ABO_3 structure are expected to be vacancies.[19,25,26] Positron lifetime values can by calculated using density functional theory (DFT). These have been performed for vacancy-related defects in $SrTiO_3$,[27–29] and the values obtained for relevant defects are given in Table I. The two cation vacancy lifetimes have been calculated using the relaxed near-neighbor atom geometries given by first principles studies for the −2 and −4 charge states of the Sr and Ti vacancies, respectively,[25,29] the vacancy complex lifetime used unrelaxed atomic positions.[28]

II. EXPERIMENT

$SrTiO_3$ films were deposited by PLD on $SrTiO_3$ (001) substrates using a KrF excimer laser, and the laser fluence was varied between 1.00 and 2.50 J cm^{-2}. Films were grown in 0.25 mbar oxygen with a substrate temperature of 720 °C, and then cooled in 0.25 mbar oxygen. The rate per laser shot was ~0.03 nm at 2.00 J cm^{-2}, and the films were ~200 nm thick. Atomic force microscopy showed that the 1.67–2.50 J cm^{-2} films exhibited smooth step-terrace structure, confirming layer-by-layer growth, and lower fluence values resulted in island growth. The c-axis lattice parameter expansion was determined by fitting the $SrTiO_3$ (002) x-ray diffraction (XRD) Cu-$K_{\alpha 1}$ peaks for the substrate and the film using Voigt functions.[6,29]

Lamella specimens for (S)TEM investigations were prepared by focused ion beam (FEI Helios NanoLab 400S). These samples were further thinned, to be sufficiently transparent to electrons, by Ar-ion milling in a Bal-Tec Res-120 system. Damage layers resulting from these processes were removed using a Nanomill system. HRTEM investigations were performed using an FEI Titan 80-300 microscope equipped with a spherical aberration correction system for the objective lens. HAADF images were recorded on an FEI Titan 800-300 scanning transmission electron microscope equipped with a spherical aberration corrector for the electron probe. Both microscopes were operated at 300 kV.

Variable-energy (VE) PALS measurements were performed on films grown with laser fluences in the range 1.17–2.00 J cm^{-2} at the neutron induced positron source (NEPOMUC) at the Munich research reactor FRMII.[30,31] The positron beam energy was varied between 1 to 18 keV, and each lifetime spectra contained $>5 \times 10^6$ counts accumulated with a count rate of $\sim 6 \times 10^3$ s^{-1}. The instrument timing resolution function was normally described by three dominant, energy-dependent, terms; these showed a mean width, averaged over all energies, of 299(20) ps.

III. RESULTS AND DISCUSSION

The variation of film c-axis lattice expansion, Δc, with respect to the substrate value of 390.5 pm, as a function of laser fluence, F, is shown in Figs. 2 and 4, where the form of the variation is consistent with that observed in previous studies. The optimal fluence, F_o, was found to be 1.50 J cm^{-2}, and resulted in films with c-axis lattice parameters coincident with the substrate. Films grown with fluences in the range 1.17–2.00 J cm^{-2} were measured using VE-PALS, and the variations in the mean positron lifetime, τ_m, with

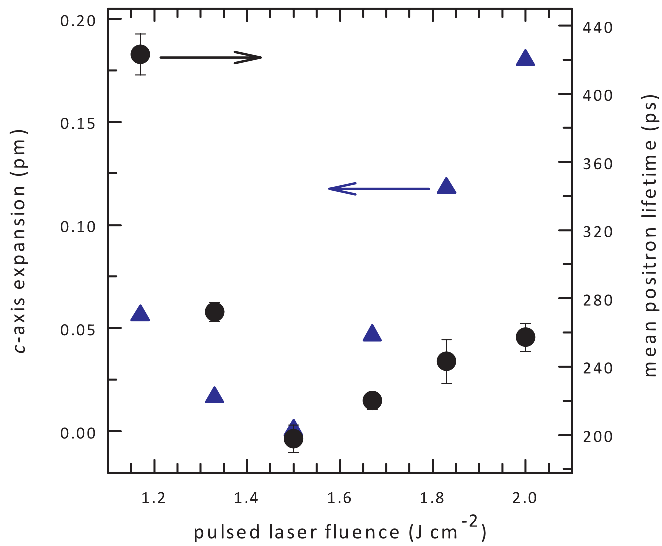

FIG. 4. (Color online) Pulsed laser deposited $SrTiO_3$ thin film out-of-plane lattice parameter expansion (up-triangle) and mean positron lifetime (circle) against laser fluence, F.

positron implantation energy, and hence mean implantation depth, are shown in Fig. 5(a). The Makhovian implantation profiles broaden with increasing energy [Fig. 5(b)]. The thin film is clearly differentiated from the substrate; the mean lifetime obtained for the substrate is ∼165 ps, consistent with values measured in bulk single crystals.[27] The values averaged over the implantation energy range for which the positrons are annihilating predominately from the films are shown in Fig. 4. The mean positron lifetimes measured in the films are all greater than the $SrTiO_3$ bulk lifetime of ∼155 ps,[27,32] indicating that positron trapping to open-volume defects occurs. The τ_m increases systematically from ∼198 ps for the film grown using F_o of 1.50 J cm^{-2} ($\Delta c \sim 0$) to 257 ps for the 2.00 J cm^{-2} film ($\Delta c \sim 0.18$ pm), which is expected to be Sr deficient. The τ_m for the optimal film is greater than the DFT calculated value for the Ti monovacancy of ∼189 ps (Table I), and hence it requires the presence of larger vacancy-related defects. The τ_m also increases with reducing F below F_o in the Ti-deficient regime. The rate of increase is markedly higher for the Ti-deficient films; it is already ∼272 ps for the 1.33 J cm^{-2} film, i.e., higher than the 2.00 J cm^{-2} sample value, and it increases to 423 ps for the 1.17 J cm^{-2} grown film. This lifetime value is significantly larger than the DFT calculated value for the Sr vacancy of ∼281 ps (Table I), and it provides direct evidence for the presence of larger vacancy defect complexes or clusters.

The $SrTiO_3$ films were further investigated by (S)TEM. Low-magnification overviews are shown in Figs. 6(a), 7(a), and 8(a) for 2.00 J cm^{-2}, 1.50 J cm^{-2}, and 1.17 J cm^{-2} grown films, and the corresponding film thicknesses were measured to be ∼170 nm, 220 nm, and 120 nm, respectively. The variation in thickness is consistent with the variations in the mean positron lifetime depth profiles [Fig. 5(a)]. The homogeneous image contrast seen in Figs. 6(a) and 7(a) indicates that both the 2.00 J cm^{-2}, Sr-deficient film and the film grown using F_o of 1.50 J cm^{-2} are single crystalline, as further demonstrated by the HAADF [Figs. 6(b) and 7(b)] and

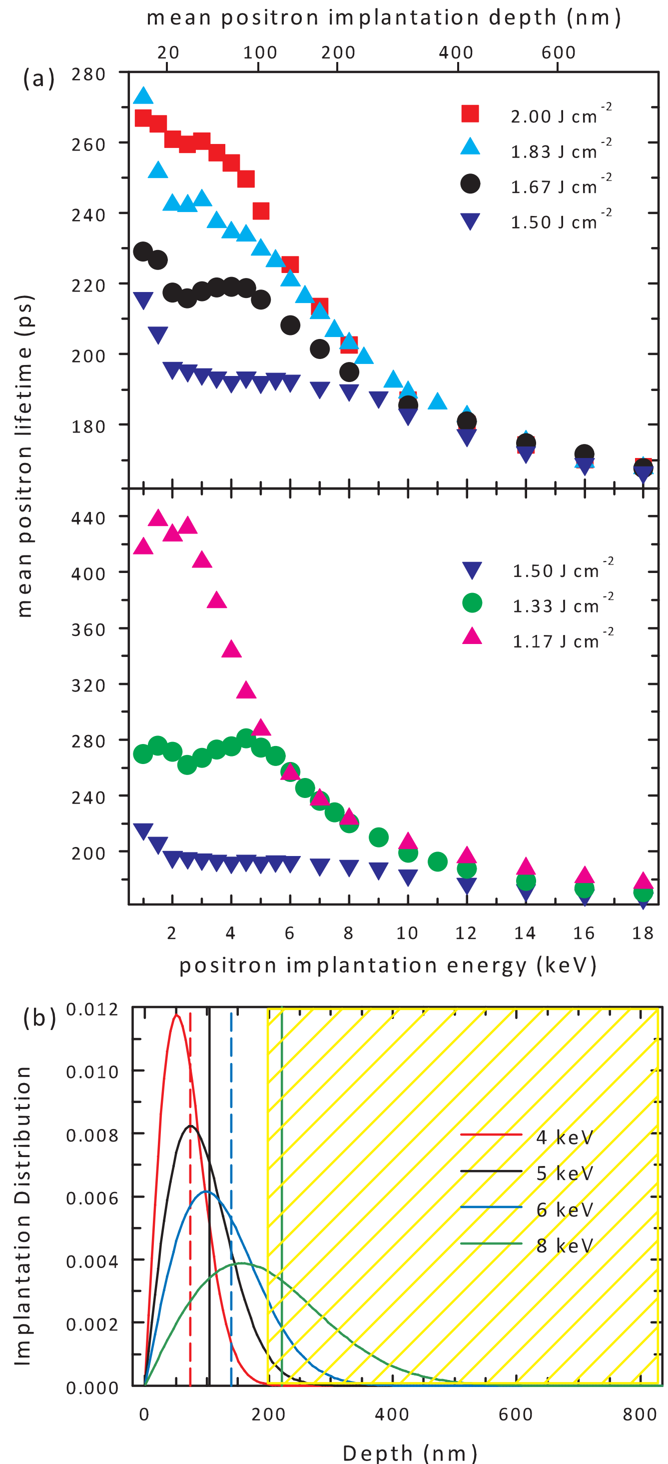

FIG. 5. (Color online) (a) Variable-energy positron annihilation lifetime spectroscopy mean lifetime against positron implantation energy for the series of PLD-grown $SrTiO_3$ thin films. (b) The Makhovian positron implantation profiles (substrate denoted by yellow shading).

HRTEM images [Figs. 6(c) and 7(c)]. For all of the regions investigated, neither extended lattice defects (i.e., dislocations, planar defects) nor obvious composition segregations were observable for either film. Further, there was no evidence for wide-area inhomogeneous contrast modulations in the

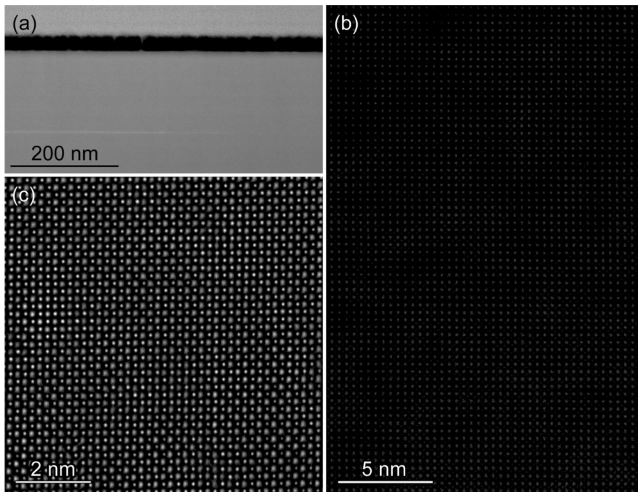

FIG. 6. (a) Low-magnification overview, (b) HAADF, and (c) HRTEM images of $SrTiO_3$ film grown using a fluence of 2.00 J cm^{-2}.

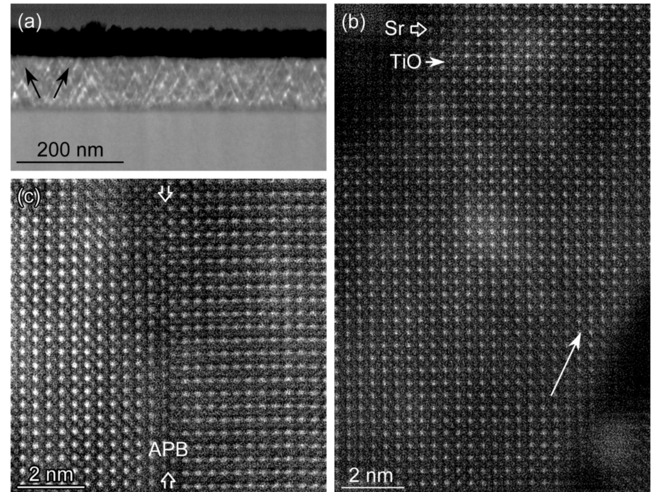

FIG. 8. (a) Low-magnification overview and (b), (c) HAADF images of the $SrTiO_3$ film grown using 1.17 J cm^{-2}. Inclined arrowheads in (a) and (b) show the ⟨112⟩ growth directions of $SrTiO_3$ grain.

2.00 J cm^{-2} ($F/F_o \sim 1.3$) grown film ($\Delta c \sim 0.18$ pm) images (Fig. 6). These have been observed previously for Sr-deficient thin films,[8,11,17] for example, for a PLD film grown with a high fluence ($F/F_o \sim 6.3$) giving Ti/Sr ∼1.04 and a 5 pm lattice expansion.[8]

In contrast, the Ti-deficient region film grown using 1.17 J cm^{-2} shown in Fig. 8(a) exhibits a microstructure of highly ⟨001⟩ textured $SrTiO_3$ grains growing along equivalent ⟨112⟩ directions [as indicated by the inclined arrowhead in Figs. 8(a) and 8(b)]. The diversity of growth directions leads to a severe overlapping of grains. Small misorientation angles between these grains are also found. Figure 8(b) shows a HAADF image of one of these grains. The heavier Sr column shows a brighter contrast, while the TiO columns are much weaker (see horizontal arrowheads). Parts of two further grains can also be seen at the top-left and bottom-right corners. However, their lattices are blurred due to the misorientation. Furthermore, planar defects, lying in {100} planes, were frequently observed in this film (from HRTEM images recorded

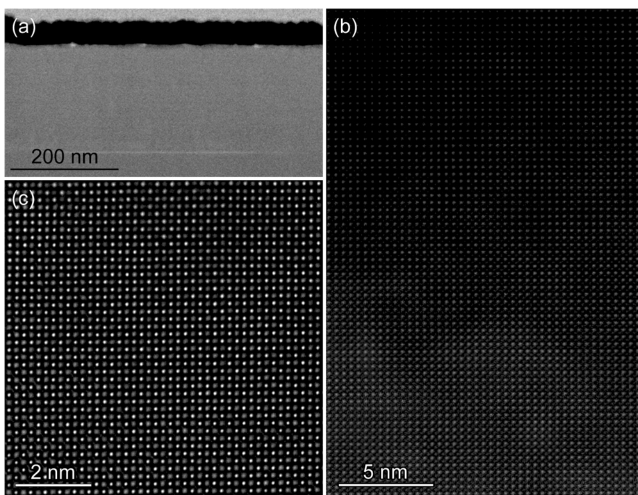

FIG. 7. (a) Low-magnification overview, (b) HAADF, and (c) HRTEM images of $SrTiO_3$ film grown using a fluence of 1.50 J cm^{-2}.

from conventionally prepared plan-view sample and focused ion beam prepared lamellae, not shown here). An example is displayed in HAADF image in Fig. 8(c), where an antiphase boundary (APB) is observed and a displacement across the boundary of 1/2 ⟨001⟩ was measured. It can be seen that a TiO_2 layer was missing at the APB, resulting in a local structure with a double SrO layer RP phase.

Further insight on the nature of the vacancy-related defects present in the films can be obtained from deconvolving the VE-PALS spectra, so resolving multiple positron states. The spectra from the films grown with fluences in the range $1.50 \leqslant F \leqslant 2.00$ J cm^{-2} were fitted using three positron lifetime components; however, the third component had an intensity less than 0.3% and is not shown. The near-surface regions of the films, up to approximately 3 keV (∼40 nm), typically showed a second lifetime value greater than ∼280 ps, indicating a contribution from larger vacancy complex defects. Up to 5 keV, the implantation profiles were confined within the ∼200 nm films [Fig. 5(b)]; as the implantation energy increased, the contribution from the substrate systematically increased, causing a reduction in the resolved lifetime values (Fig. 9). Positrons implanted with energies in the range 3–5 keV profile through the bulk of the thin film, and the two dominant lifetime component values were found to be approximately constant, e.g., Fig. 9(a). The average values for lifetimes and intensities for the sequence of films are shown in Fig. 10. Two vacancy defect lifetimes, ∼280 ps and ∼181 ps, were clearly resolved [Fig. 10(a)] for all the films, and they are in good agreement with crystal $SrTiO_3$ measurements and the DFT lifetime values for V_{Sr} and V_{Ti}, respectively (Table I).[27,29] The uncertainties in fit components shown in Fig. 10 varied in accord with the intensity of trapping to V_{Sr} and V_{Ti} defects; the intensity of trapping to Sr vacancies was smallest for the 1.50 J cm^{-2} film as also seen in Fig. 11, and the uncertainty in the associated lifetime of this component was the greatest [see Figs. 10, 11(a), and 11(b)]. Additional deconvolution fits were performed for this film where the lifetime value of one component was constrained to the V_{Sr} value, 281 ps, and the results are shown in Figs. 11(c)

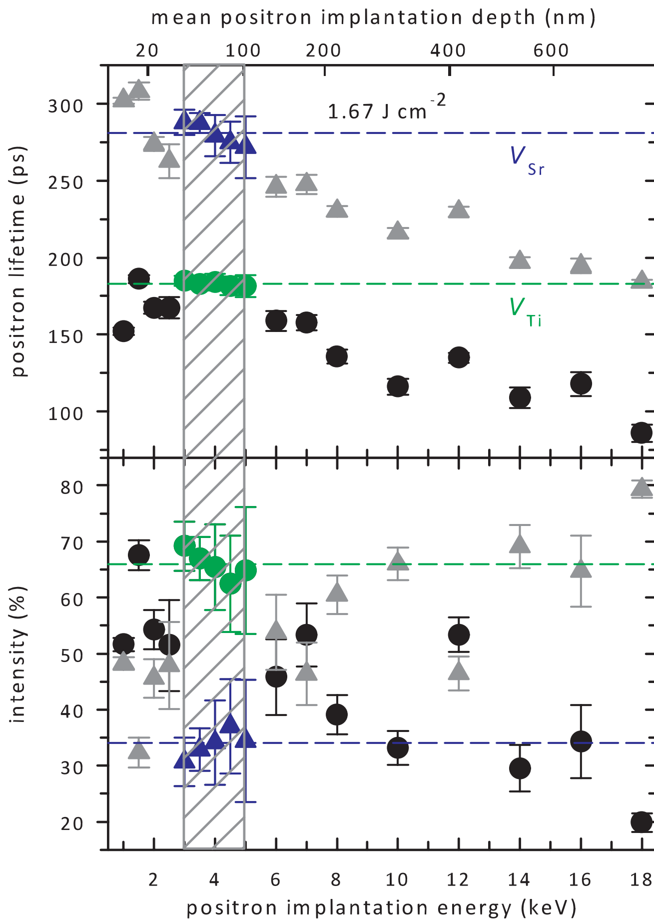

FIG. 9. (Color online) Depth profiled positron lifetime components for the 1.67 J cm^{-2} $SrTiO_3$ film, showing the lifetimes (dashed lines denote 181 and 281 ps) and associated intensities against positron implantation energy. The 3–5 keV range is highlighted (gray shading).

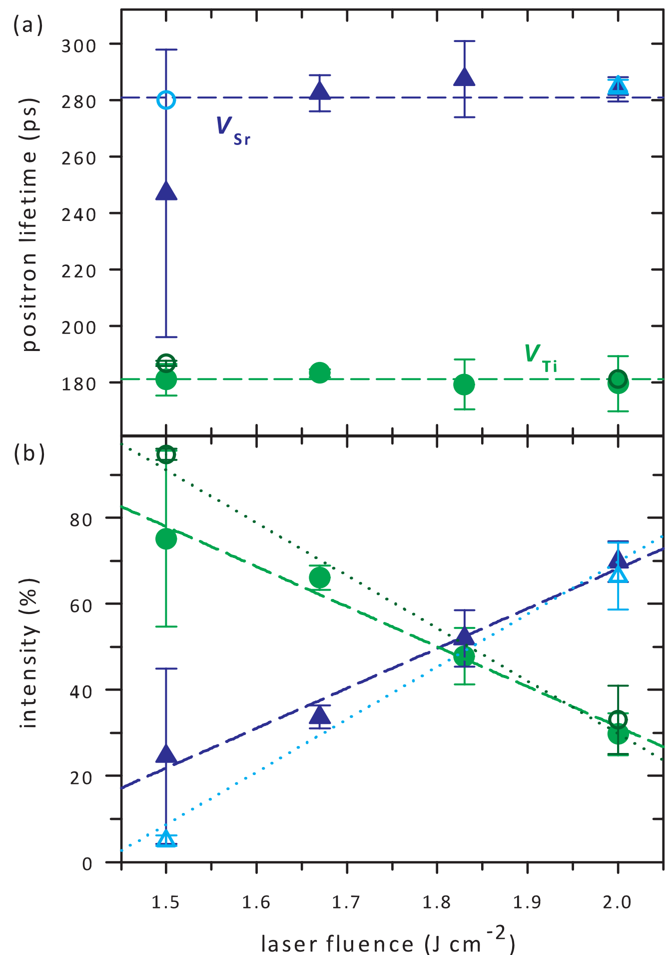

FIG. 10. (Color online) The two-component free-fit positron lifetimes (a) and intensities (b) for the 1.50–2.00 J cm^{-2} films (3–5 keV average). The V_{Ti} and V_{Sr} lifetimes 181 ps and 281 ps, respectively, are also shown (dashed) in (a). The constrained fit results for the 1.50 J cm^{-2} and the 2.00 J cm^{-2} films are shown as open symbols.

and 11(d) and in Fig. 10 (open symbols). The V_{Ti} lifetime value was obtained for the unconstrained component, and the uncertainties were markedly reduced (the fit variance was slightly reduced compared to the free fit). Similar fits were performed for the 2.00 J cm^{-2} film, constraining one lifetime to 181 ps; the results are also shown in Fig. 10 (open symbols).

Saturation trapping to vacancy defects was observed in all films. Vacancy defect concentrations exceeded the limit defined by $\mu_d [d]_{\mathrm{Sat}} \tau_b \approx 10$. There have been no direct determinations of a defect-specific trapping coefficient in an oxide, so the values obtained for negative charge state vacancies in semiconductors have been typically used.[24,27,29] However, a lower limit for $\mu(V_{Sr})$ can be estimated from the results of a recent VE-PALS study of MBE-grown La-doped $SrTiO_3$ thin films where positron trapping to vacancies was below the saturation trapping limit, allowing the positron trapping rate to V_{Sr} defects to be estimated.[32] Cation vacancies are expected to act as acceptor defects, and previous studies had established a one to one relation between [La] and the resulting carrier density through the [La] range $\sim 5 \times 10^{17}$ cm^{-3} to $\sim 3 \times 10^{20}$ cm^{-3} for the films.[33] Hence, considering the [La] $\sim 8 \times 10^{17}$ cm^{-3} film measured by VE-PALS,[32] if it assumed that $[V_{Sr}] \leqslant 8 \times 10^{16}$ cm^{-3}, a lower limit for $\mu(V_{Sr})$ of $\sim 3 \times 10^{15}$ s^{-1} is obtained. This suggests that the threshold concentration of cation vacancy defects above which saturation trapping is expected is of the order estimated earlier, ~20–50 ppm.

From the variation of Ti/Sr with Δc (Fig. 1), and the behavior of Δc with F (Figs. 2 and 4), it is expected that the film grown with optimal fluence, 1.50 J cm^{-2}, and exhibiting a $\Delta c \sim 0$ should have Ti/Sr = 1.0, yet the VE-PALS results given in Figs. 10 and 11 show that saturation trapping occurred and that positron trapping was dominated by Ti vacancy defects. These observations can be consistent, given markedly higher sensitivity of positron annihilation spectroscopy compared to EDX. The existence of saturation trapping and the dominance of positron trapping to V_{Ti} for the nominally stoichiometric film would be consistent with [Ti] ≈ [Sr] if $[V_{Ti}] \approx [V_{Sr}]$, if these concentrations were approximately in the range ~20–1000 ppm (assuming EDX precision of 0.1%). Further, it would require the positron defect-specific trapping coefficient for Ti vacancies, $\mu(V_{Ti})$ to be greater than $\mu(V_{Sr})$ [see Eq. (2)]. A higher trapping coefficient from B-site vacancies compared to A-site vacancies may be expected given the higher local negative charge with respect to the lattice, assuming an ionic

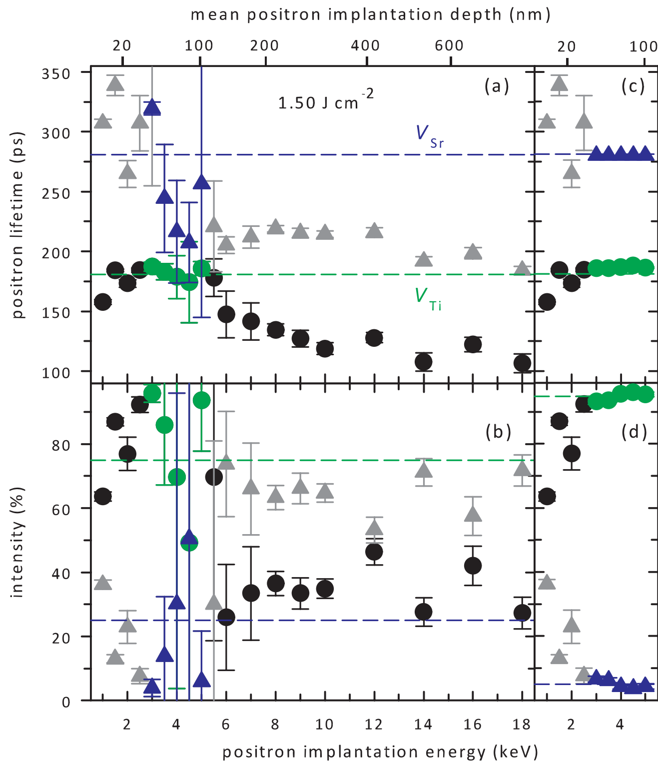

FIG. 11. (Color online) Depth profiled free-fit positron lifetime components for the 1.50 J cm^{-2} $SrTiO_3$ film, showing the lifetimes (a) (dashed lines denote 181 and 281 ps) and associated intensities (b) against positron implantation energy. The fit results obtained by fixing one lifetime value at 281 ps for the range 3–5 keV are shown in (c) and (d).

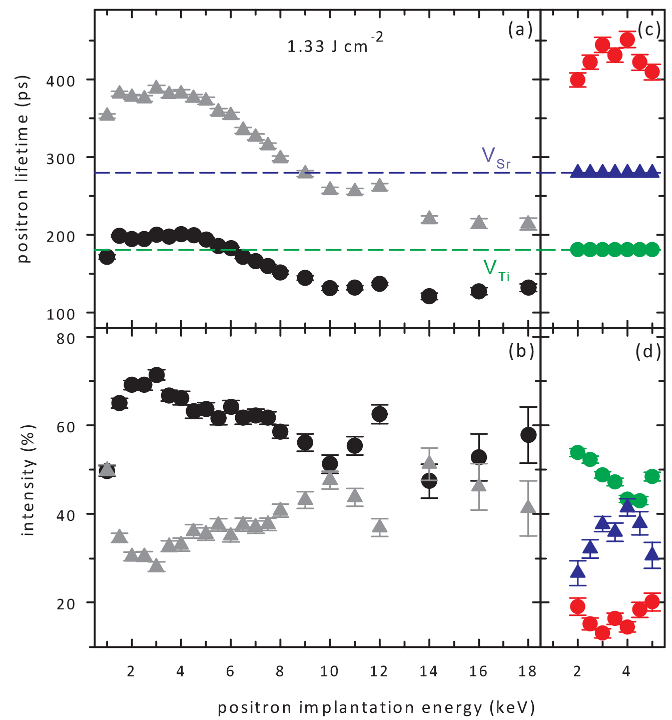

FIG. 12. (Color online) Depth profiled free-fit positron lifetime components for the 1.33 J cm^{-2} $SrTiO_3$ film, showing the lifetimes (a) (dashed lines denote 181 and 281 ps) and associated intensities (b) against positron implantation energy. The fit results obtained by fixing two lifetime values, 181 ps and 281 ps, for the implantation range confined to the film, are shown in (c) and (d).

model −4 compared to −2 (V_{Ti}^{4-},V_{Sr}^{2-}). Evidence for $\mu(V_B) > \mu(V_A)$ has been obtained previously from the temperature dependence of positron trapping in single-crystal and ceramic perovskite oxides.[27,34] Further, from Eq. (2), if it is assumed that $[V_{Ti}] = [V_{Sr}]$, then $\mu(V_{Ti})/\mu(V_{Sr})$ is equal to the ratio of the component intensities, $I(V_{Ti})/I(V_{Sr})$, shown in Figs. 10(b) and 11(b), which for the free fit is ∼3 (3.6 using the linear trend values), but this increases to ∼19 if the constrained fit results are used [Figs. 10(b) and 11(d)]. The former is a plausible value for the ratio of trapping coefficients; however, the latter is larger than expected and would then suggest $[V_{Ti}] > [V_{Sr}]$.

The systematic increase in the intensity of the V_{Sr} lifetime component with laser fluence shown in Fig. 9(b) is consistent with the expected increase in Sr deficiency (Figs. 1 and 2). From Eq. (2), the ratio $[V_{Sr}]/[V_{Ti}]$ increases for the fluence range 1.50–2.00 J cm^{-2} from approximately 7 (free-fit results) to 38 (single constraint fit results). From Figs. 1 and 2, the increase in Ti/Sr over this fluence range should be resolved by EDX. In consequence, despite the lower defect-specific trapping rate for V_{Sr}, a far more marked increase in the $[V_{Sr}]/[V_{Ti}]$ leading to a complete suppression of V_{Ti} trapping may have been expected. The single-crystal quality and lack of any discernible differences in the HAADF images from the 1.50 J cm^{-2} and 2.00 J cm^{-2} films shown in Figs. 7 and 6 contrast with the clear differences in vacancy defect content observed by VE-PALS.

The results obtained from the Ti-deficient films were found to be quite different from the systematic trends observed for the Sr-deficient sequence. Comparison of the TEM images of the 1.50 J cm^{-2} and 1.17 J cm^{-2} grown films, given in Figs. 7 and 8, shows that the microstructure changed markedly from single crystal to one showing texture and the presence of additional SrO layers forming RP planar defects. The VE-PALS mean lifetime profiles [Fig. 5(a)] show a similar rapid change. The τ_m, averaged through the film (Fig. 4), increased from 198 ps to 272 ps between the 1.50 J cm^{-2} and 1.33 J cm^{-2} grown films, i.e., greater than the 2.00 J cm^{-2} Sr-deficient film value of 257 ps. It then rose to 423 ps for the 1.17 J cm^{-2} grown sample. A τ_m of this value requires the presence of a vacancy-related defect larger than Sr monovacancies, such as vacancy complexes or vacancy clusters. The deconvolved spectra, free-fitting to three components, are shown for the 1.33 J cm^{-2} grown film in Figs. 12(a) and 12(b) and for the 1.17 J cm^{-2} grown film in Figs. 13(a) and 13(b), and the very weak longest lifetime component for both films is shown in Fig. 14. Figures 12(a), 12(b), 13(a), and 13(b) show that a significant lifetime component with a value greater than the Sr vacancy lifetime is present in both films. In addition, the values of the first lifetime components suggest that trapping to V_{Ti} dominates for the 1.33 J cm^{-2} grown film, while trapping to V_{Sr} defects contributed for the 1.17 J cm^{-2} grown film. However, the component lifetime values are not in precise agreement between films, or with the values obtained from the 1.50–2.00 J cm^{-2} sequence of films (Fig. 10).

Further insight was obtained by performing four-component fits, constraining two component lifetimes at the V_{Ti} and V_{Sr} values; these are shown in Figs. 12(c), 12(d),

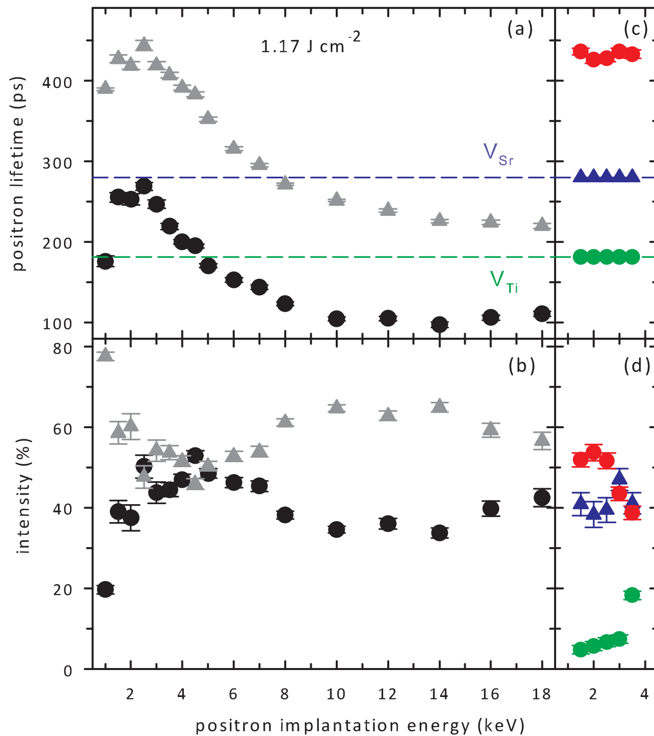

FIG. 13. (Color online) Depth profiled free-fit positron lifetime components for the 1.17 J cm^{-2} $SrTiO_3$ film, showing the lifetimes (a) (dashed lines denote 181 and 281 ps) and associated intensities (b) against positron implantation energy. The fit results obtained by fixing two lifetime values, 181 ps and 281 ps, for the implantation range confined to the film, are shown in (c) and (d).

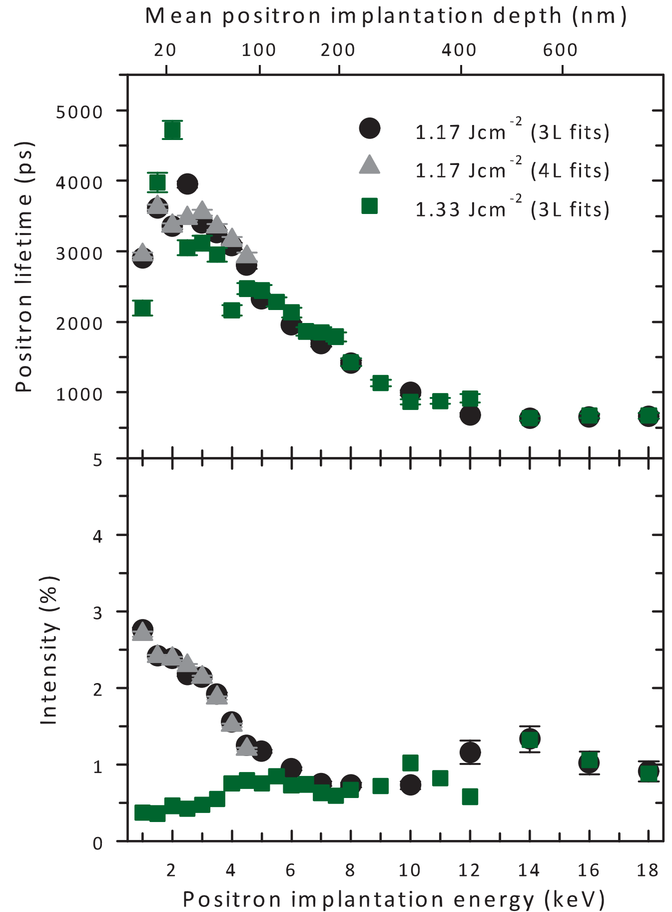

FIG. 14. (Color online) Depth profiled long-lifetime component results for the 1.17 J cm^{-2} and 1.33 J cm^{-2} $SrTiO_3$ films, showing the lifetimes and associated intensities. Values from both three-component free fits (circle) and four-component fits with two fixed as 181 ps and 281 ps (up-triangle) are given for the 1.17 J cm^{-2} sample.

13(c), and 13(d) for the 1.33 J cm^{-2} and 1.17 J cm^{-2} films, respectively. These gave a third component lifetime at 430(16) ps (I_3 ∼16[3]%) and 432(5) ps (I_3 ∼48[6]%), respectively. The observation of an ∼430 ps defect lifetime is consistent with previous positron lifetime studies on $SrTiO_3$. A VE-PALS study of a PLD-grown $SrTiO_3$ thin film, exhibiting a columnar microstructure,[35,36] resolved a second lifetime at ∼407(10) ps (I_2 ∼ 13[1]%) from a three-component free-fit deconvolution, present through the body of the film.[28] A recent study of two La-doped MBE-grown $SrTiO_3$ thin films also observed positron trapping to a defect lifetime component in the range ∼370–420 ps in the near-surface (⩽50 nm) regions.[32] Further, a lifetime component at 430(10) ps has also been reported from a VE-PALS measurement of a strongly oxygen depleted Nb-doped $SrTiO_3$ substrate behind an ∼30 nm MBE-grown $BaTiO_3$ layer.[37] The DFT calculated lifetime for a Schottky defect consisting of both V_{Ti} and V_{Sr} with three nearest neighbor oxygen vacancies has been given as 316 ps.[28] Vacancy clustering has also been studied in silicon, wherein the positron lifetime systematically increases with the number of vacancies, a value of 355 ps has been reported for a five vacancy cluster,[38] and lifetimes in the range 420–430 ps have been associated with vacancy clusters containing between 10 and 14 vacancies.[39] Recently, atomic-resolution scanning tunneling microscopy images of processed $SrTiO_3$(001) surfaces have shown Ti_4O_3 vacancy cluster defects in the surface Ti terminated surface.[40] Similar embedded vacancy clusters, possibly also including Sr vacancies, would be of comparable size to the defects detected here.

The success of the four-term fits, with two constrained lifetimes at the V_{Ti} and V_{Sr} values, in consistently identifying the presence of a vacancy cluster defect at ∼430 ps, combined with slightly lower chi-squared values for these fits, suggests that these are physically plausible. It is not always possible to uniquely deconvolve lifetime components; this can occur if two physical components are too close in lifetime, $\tau_n < \sim 1.5\tau_{n+1}$, and it can depend of the number and intensities of the components. In fact, the condition on the closeness of resolvable lifetime components is further weakened if the number of components in the spectrum increases. Constraining one or more values in the fitting process imposes a model, but if this reduces chi-squared, and yields consistent results across of sequence of samples, a degree of confidence in the plausibility of the model can accrue.

Reviewing again the three-term unconstrained deconvolution of the 1.33 J cm^{-2} grown Ti-deficient sample lifetime spectra, these resulted in a dominant component at ∼195 ps (I_1 ∼ 70%), shown in Figs. 12(a) and 12(b). Comparing this value to the DFT calculated lifetimes for vacancy defects in $SrTiO_3$ (Table I), and considering the strong experimental

evidence that V_{Ti} has a lifetime of ∼181 ps and V_{Sr} has a lifetime of 281 ps, leads to the conclusion that the ∼195 ps component is the weighted average of two or more unresolved terms. The closeness of the value to V_{Ti} provides good evidence that trapping to this defect dominates, and the inclusion of the fixed component at 181 ps is justified. Identifying the other vacancy defects responsible for the increase in the weighted average from 181 ps to 195 ps is less straightforward. The two physically plausible possibilities are the presence of V_{Sr} defects, or of V_{Ti}-nV_O defects (Table I). While populations of V_{Sr} and V_{Ti} defects can be resolved from each other, as directly demonstrated for the Sr-deficient samples described above, this was possible because there were only two dominant lifetime components in the spectra. For the Ti-deficient films, there are three or more separate vacancy defect components; in consequence, it is not possible to directly separate V_{Sr} and V_{Ti} terms. This has been observed previously for $SrTiO_3$.[27,28,32]

Again, the success of the free-fit component of the four-term fits in identifying the ∼430 ps vacancy cluster defects provides evidence that the three-term free-fit second lifetime component at ∼380 ps Figs. 12(a) and 12(a) also represents the weighted average of two or more unresolved components. The possible vacancy defects with lifetimes in the appropriate range of ∼280–430 ps include V_{Sr} defects and V_{Sr} complexes with oxygen vacancies and Ti vacancies.

In consequence, four-term fits, with two lifetimes fixed as the values of V_{Sr} and V_{Ti}, shown in Figs. 12(c) and 12(d), represent the simplest constrained four-term deconvolution model for the 1.33 J cm^{-2} grown sample lifetime spectra. Further, if four-term fits are performed fixing two lifetimes at 181 ps and 430 ps, results similar to Figs. 12(c) and 12(d) are obtained with a second component lifetime of 281(15) ps. These lifetime values provide evidence that positron trapping to the Ti-deficient 1.33 J cm^{-2} grown film is dominated by V_{Ti} defects, but there are significant contributions from V_{Sr} defects and from vacancy clusters.

For the more strongly Ti-deficient, 1.17 J cm^{-2} grown film, the three-term free fits shown in Fig. 13 already provided evidence for the presence of a lifetime component with a value close to the Sr vacancy, and one at ∼430 ps. Attempts to constrain four-term deconvolutions using fixed lifetimes other than 281 ps gave physically implausible results. The fits shown in Fig. 13 provide evidence that positron trapping is dominated by Sr vacancy–related defects and by the vacancy cluster defect with a lifetime of ∼430 ps; there is also evidence for a residual contribution from V_{Ti} defects.

Figure 14 shows the values for the longest lifetime component obtained from the deconvolution fits of the 1.33 J cm^{-2} and 1.17 J cm^{-2} films; a similar component is obtained from the fits of the Sr-deficient films but is always of negligible intensity (<0.3%). However, for the 1.17 J cm^{-2} sample, a lifetime component at ∼3.5 ns and intensity ∼2.5% is clearly resolved from the region of the film. This is a lifetime component resulting from the formation of positronium in a large open volume, such as nanovoids; the confined ortho-positronium can annihilate by interacting with electrons at the void surface.[24] A simple quantum mechanical model can be used to estimate the size, assuming spherical shape, and it predicts that a 3.5 ns lifetime corresponds to a nanovoid diameter of ∼0.8 nm.[41]

In summary, the two Ti-deficient films show positron trapping to an open-volume defect with a lifetime of 430(10) ps, and DFT calculations provide evidence that this is a vacancy cluster that is larger than a Schottky defect, possibly containing on the order of ten vacancies. The previous observation of this defect in the near-surface region of high-quality epitaxial $SrTiO_3$ films,[32] and of a Nb-doped $SrTiO_3$ substrate,[37] suggests that the defect is present in the bulk rather than associated with the grain boundaries or RP regions. The intensity of trapping to the vacancy cluster increases with decreasing laser fluence, and hence increasing Ti deficiency. The majority of the lifetime spectrum intensity remains associated with positron trapping to cation vacancy-related defects, and this reduces from ∼84% for the 1.33 J cm^{-2} film to ∼50% for 1.17 J cm^{-2} film. It is dominated by V_{Ti} defects in the former (Figs. 12(c) and 12(d), but by Sr vacancies in the latter [Figs. 13(c) and 13(d)]. Further, a positronium component was detected in the 1.17 J cm^{-2} film (Fig. 14), indicating the presence of a larger open volume with a diameter of ∼0.8 nm. TEM shows this film was textured and contained RP planar defects (Fig. 8) and suggests that these large open volume defects are associated with the change in microstructure.

Deviations between thin film and target stoichiometry for pulsed laser deposited thin films are basically a result of two effects, namely, incongruent ablation and preferential scattering of lighter ablated species during their motion towards the substrate in the O_2 background gas.[42] On the one hand, a progressive preferential ablation of the Ti species with increasing laser fluence leads to a regime of Ti-rich thin film growth at larger fluences. On the other hand, in the low-laser-fluence regime, a more effective scattering of the lighter Ti plume species results in Sr-rich films. The accommodation of the Sr excess is primarily in the form of incorporation of SrO layers in RP defects, but this is accompanied by vacancy cluster defect formation and by cation monovacancy defects. There is an increase in positron trapping to cluster defects with increasing Sr excess, and, interestingly, the associated cation vacancy defect type changes from the expected Ti vacancies to Sr vacancies with increasing Sr excess. Presumably, this occurs because there is a capacity for formation of extra SrO layers in RP defects to slightly overcompensate the nonstoichiometry. It has previously been proposed that Sr antisite oxygen vacancy complexes, Sr_{Ti}-V_O, acted as precursor defects for RP defect formation and explained the lattice expansion in this Ti-deficiency regime.[16] However, despite the reported high formation energy,[19] here Ti vacancies are directly observed for small Ti deficiency. For the Ti-rich regime studied, high crystalline quality is retained, and PALS only detected cation monovacancy defects at concentrations greater than ∼30–50 ppm. Both cation vacancies were observed; however, the fraction of trapping to Sr vacancies systematically increased with increasing Ti excess and dominated for fluences greater than ∼1.8 J cm^{-2} (Fig. 10). This is due to V_{Ti} defects having a higher positron trapping coefficient than V_{Sr} defects; nevertheless, the results do show that Ti vacancies were a minority defect present in the Sr-deficient region samples.

IV. CONCLUSIONS

A series of PLD $SrTiO_3$ thin films was grown using increasing laser fluence. The out-of-plane lattice parameter

expansion, Δc, with respect to the $SrTiO_3$ substrate value decreased to $\Delta c = 0.0$ for the optimal fluence of 1.50 J cm^{-2}, and then increased again for high fluences. This is in agreement with earlier work that also established that films grown with fluences lower than the optimum are Ti deficient, while those grown with higher values are Sr deficient. A detailed study using HRTEM, STEM, and VE-PALS was performed on films grown with laser fluences in the range 1.17 J cm^{-2} to 2.00 J cm^{-2}.

The series of films grown using fluences in the range 1.50–2.00 J cm^{-2} varied from the optimum value giving a film with $\Delta c = 0.0$, into the Sr-deficient region where the 2.00 J cm^{-2} film showed a $\Delta c = 0.18$ pm. The TEM images were similar for the 1.50 J cm^{-2} and 2.00 J cm^{-2} films; both were crystalline with no evidence of lattice disorder. However, the VE-PALS results showed trapping to two vacancy defects, one with a lifetime of ~181 ps and one at 281 ps. DFT calculations identify these as the Ti vacancy and the Sr vacancy, respectively. The defect concentrations were higher than the threshold for saturation of positron trapping, which was estimated to be ~20–50 ppm, for all the films studied. In consequence, sensitivity to absolute concentrations is lost, but if more than one defect is present, information on the ratio of concentrations can in principle be obtained. The optimal 1.50 J cm^{-2} grown film showed positron trapping dominated by V_{Ti} defects. The film is expected to have Ti/Sr = 1; hence if $[V_{Sr}] = [V_{Ti}]$, the dominance of trapping to the V_{Ti} defect provides evidence that the defect-specific trapping coefficient for the nominal -4 charge state B-site vacancy is greater than that for the -2 charge A-site vacancy. Here, fitting of the PALS spectra was performed using both free and fixed components to provide a more objective range for the ratio of defect-specific trapping coefficients between A-site and B-site monovacancy defects. The cation vacancy concentration ratio $[V_{Sr}]/[V_{Ti}]$ systematically increases with laser fluence through the 1.50–2.00 J cm^{-2} range. These measurements directly show that nonstoichiometry is accommodated by the formation of Sr vacancies for this range of laser fluence. However, presumably due to kinetic limitations, the suppression of V_{Ti} defects with increasing Ti/Sr is less rapid than expected.

Films grown with lower than optimal laser fluence in the Ti-deficient region show a slower increase in Δc with changing fluence, yet they exhibit a marked change in microstructure. HRTEM clearly illustrates that with decreasing fluence, and hence Ti/Sr, a primary mechanism for the accommodation of nonstoichiometry is the insertion of additional SrO layers in RP planar defects. PALS shows that this is accompanied by the formation of vacancy cluster defects, larger than Schottky defects, containing of the order of 10–14 vacancies, and characterized by a lifetime of ~430 ps. Similar size cluster defects have also been observed in the surface of $SrTiO_3$ by STM.[40] Further, there is rapid change in the accompanying cation vacancies. It is interesting to note that in the 1.33 J cm^{-2} grown film, these are, despite the reported high formation energy,[19] primarily Ti vacancies. In the 1.17 J cm^{-2} grown film, however, where TEM clearly shows RP planar defects, and texture, Ti vacancies are suppressed, but V_{Sr} defects are observed. Positron lifetime measurements also observe positronium formation and annihilation, and suggest this is occurring from nanovoids estimated to have diameters of ~0.8 nm in this film. Accommodation of Ti deficiency is observed to involve the well-known formation of additional SrO layers as RP planar defects, but unexpectedly this can be offset by Sr vacancy formation, and further vacancy cluster formation is also observed.

Advances in understanding of morphology development during PLD growth have been made;[43] however, stoichiometry of the deposited layers also depends on the laser plume composition and dynamics,[42] and while DFT-aided analysis of near-equilibrium defect modeling has provided limited insight for PLD films,[13] developing appropriate combined modeling capable of predicting point defect contents of PLD-grown complex oxide films remains challenging.

ACKNOWLEDGMENTS

D.J.K. acknowledges European Commission Programme (RII3-CT-2003-505925). This work has been supported in parts by the Deutsche Forschungsgemeinschaft (SFB 917). We thank C. Hugenschmidt for providing the NEUPOMUC beamline. We thank D. Meertens and W. Sybertz, Forschungszentrum Jülich, for preparing the TEM/STEM specimens.

*Corresponding authors: d.j.keeble@dundee.ac.uk; r.dittmann@fz-juelich.de

[1] E. Bousquet, M. Dawber, N. Stucki, C. Lichtensteiger, P. Hermet, S. Gariglio, J. M. Triscone, and P. Ghosez, Nature **452**, 732 (2008).
[2] A. Ohtomo and H. Y. Hwang, Nature **427**, 423 (2004).
[3] J. Mannhart and D. G. Schlom, Science **327**, 1607 (2010).
[4] H. Takagi and H. Y. Hwang, Science **327**, 1601 (2010).
[5] B. Dam, J. H. Rector, J. Johansson, J. Huijbregtse, and D. G. De Groot, J. Appl. Phys. **83**, 3386 (1998).
[6] T. Ohnishi, M. Lippmaa, T. Yamamoto, S. Meguro, and H. Koinuma, Appl. Phys. Lett. **87**, 241919 (2005).
[7] T. Ohnishi, H. Koinuma, and M. Lippmaa, Appl. Surf. Sci. **252**, 2466 (2006).
[8] T. Ohnishi, K. Shibuya, T. Yamamoto, and M. Lippmaa, J. Appl. Phys. **103**, 103703 (2008).
[9] Y. Kozuka, Y. Hikita, C. Bell, and H. Y. Hwang, Appl. Phys. Lett. **97**, 012107 (2010).
[10] Y. Tokuda, S. Kobayashi, T. Ohnishi, T. Mizoguchi, N. Shibata, Y. Ikuhara, and T. Yamamoto, Appl. Phys. Lett. **99**, 173109 (2011).
[11] Y. Tokuda, S. Kobayashi, T. Ohnishi, T. Mizoguchi, N. Shibata, Y. Ikuhara, and T. Yamamoto, Appl. Phys. Lett. **99**, 033110 (2011).
[12] E. Breckenfeld, R. Wilson, J. Karthik, A. R. Damodaran, D. G. Cahill, and L. W. Martin, Chem. Mater. **24**, 331 (2012).
[13] E. Ertekin, V. Srinivasan, J. Ravichandran, P. B. Rossen, W. Siemons, A. Majumdar, R. Ramesh, and J. C. Grossman, Phys. Rev. B **85**, 195460 (2012).
[14] G. Eres, J. Z. Tischler, C. M. Rouleau, P. Zschack, H. M. Christen, and B. C. Larson, Phys. Rev. B **84**, 195467 (2011).
[15] A. Sambri, S. Amoruso, X. Wang, M. Radovic, F. M. Granozio, and R. Bruzzese, Appl. Phys. Lett. **91**, 151501 (2007).

[16]D. Fuchs, M. Adam, P. Schweiss, S. Gerhold, S. Schuppler, R. Schneider, and B. Obst, J. Appl. Phys. **88**, 1844 (2000).
[17]C. M. Brooks, L. F. Kourkoutis, T. Heeg, J. Schubert, D. A. Muller, and D. G. Schlom, Appl. Phys. Lett. **94**, 162905 (2009).
[18]G. Z. Liu, Q. Y. Lei, and X. X. Xi, Appl. Phys. Lett. **100**, 202902 (2012).
[19]C. R. A. Catlow, Z. X. Guo, M. Miskufova, S. A. Shevlin, A. G. H. Smith, A. A. Sokol, A. Walsh, D. J. Wilson, and S. M. Woodley, Philos. Trans. R. Soc. A **368**, 3379 (2010).
[20]S. Wiedigen, T. Kramer, M. Feuchter, I. Knorr, N. Nee, J. Hoffmann, M. Kamlah, C. A. Volkert, and C. Jooss, Appl. Phys. Lett. **100**, 061904 (2012).
[21]D. W. Oh, J. Ravichandran, C. W. Liang, W. Siemons, B. Jalan, C. M. Brooks, M. Huijben, D. G. Schlom, S. Stemmer, L. W. Martin, A. Majumdar, R. Ramesh, and D. G. Cahill, Appl. Phys. Lett. **98**, 221904 (2011).
[22]T. Suzuki, Y. Nishi, and M. Fujimoto, Philos. Mag. A **80**, 621 (2000).
[23]R. J. D. Tilley, J. Solid State Chem. **21**, 293 (1977).
[24]R. Krause-Rehberg and H. S. Leipner, *Positron Annihilation in Semiconductors* (Springer-Verlag, Berlin, 1999).
[25]T. Tanaka, K. Matsunaga, Y. Ikuhara, and T. Yamamoto, Phys. Rev. B **68**, 205213 (2003).
[26]D. M. Smyth, *The Defect Chemistry of Metal Oxides* (Oxford University Press, New York, 2000).
[27]R. A. Mackie, S. Singh, J. Laverock, S. B. Dugdale, and D. J. Keeble, Phys. Rev. B **79**, 014102 (2009).
[28]D. J. Keeble, R. A. Mackie, W. Egger, B. Löwe, P. Pikart, C. Hugenschmidt, and T. J. Jackson, Phys. Rev. B **81**, 064102 (2010).
[29]D. J. Keeble, S. Wicklein, R. Dittmann, L. Ravelli, R. A. Mackie, and W. Egger, Phys. Rev. Lett. **105**, 226102 (2010).
[30]P. Sperr, W. Egger, G. Kogel, G. Dollinger, C. Hugenschmidt, R. Repper, and C. Piochacz, Appl. Surf. Sci. **255**, 35 (2008).
[31]C. Hugenschmidt, B. Lowe, J. Mayer, C. Piochacz, P. Pikart, R. Repper, M. Stadlbauer, and K. Schreckenbach, Nucl. Instrum. Methods A **593**, 616 (2008).
[32]D. J. Keeble, B. Jalan, L. Ravelli, W. Egger, G. Kanda, and S. Stemmer, Appl. Phys. Lett. **99**, 232905 (2011).
[33]J. Son, P. Moetakef, B. Jalan, O. Bierwagen, N. J. Wright, R. Engel-Herbert, and S. Stemmer, Nature Mater. **9**, 482 (2010).
[34]D. J. Keeble, S. Singh, R. A. Mackie, M. Morozov, S. McGuire, and D. Damjanovic, Phys. Rev. B **76**, 144109 (2007).
[35]S. McGuire, D. J. Keeble, R. E. Mason, P. G. Coleman, Y. Koutsonas, and T. J. Jackson, J. Appl. Phys. **100**, 044109 (2006).
[36]Y. Y. Tse, Y. Koutsonas, T. J. Jackson, G. Passerieux, and I. P. Jones, Thin Solid Films **515**, 1788 (2006).
[37]A. Uedono, K. Shimoyama, M. Kiyohara, Z. Q. Chen, K. Yamabe, T. Ohdaira, R. Suzuki, and T. Mikado, J. Appl. Phys. **91**, 5307 (2002).
[38]M. Hakala, M. J. Puska, and R. M. Nieminen, Phys. Rev. B **57**, 7621 (1998).
[39]T. E. M. Staab, A. Sieck, M. Haugk, M. J. Puska, T. Frauenheim, and H. S. Leipner, Phys. Rev. B **65**, 115210 (2002).
[40]M. S. J. Marshall, A. E. Becerra-Toledo, L. D. Marks, and M. R. Castell, Phys. Rev. Lett. **107**, 086102 (2011).
[41]M. Eldrup, D. Lightbody, and J. N. Sherwood, Chem. Phys. **63**, 51 (1981).
[42]S. Wicklein, A. Sambri, S. Amoruso, X. Wang, R. Bruzzese, A. Koehl, and R. Dittmann, Appl. Phys. Lett. **101**, 131601 (2012).
[43]J. D. Ferguson, G. Arikan, D. S. Dale, A. R. Woll, and J. D. Brock, Phys. Rev. Lett. **103**, 256103 (2009).